Supporting Information for:

Mechanistic Origin of Photoredox Catalysis involving Iron(II) Polypyridyl Chromophores

Matthew D. Woodhouse and James K. McCusker*

Contribution from the Department of Chemistry, Michigan State University

578 South Shaw Lane East Lansing, Michigan 48824 USA

Email address: jkm@chemistry.msu.edu

Table of Contents

List of Figures:

Characterization of Benzoquinones.

General. 2,3-dichloro-5,6-dicyano-*para*-benzoquinone (DDQ) and 2,3-dicyano-*para*-hydroquinone (DCBQ) were purchased from Oakwood Chemical and used without further purification. 3,4,5,6-tetrachloro-*ortho*-benzoquinone (*o*-TCBQ) was purchased from Sigma-Aldrich and recrystallized from dilute acetic acid. 2,3,5,6-tetrachloro-*para*-benzoquinone (*p*-TCBQ) and 1,2-dihydroxybenzene were purchased from Sigma-Aldrich and used without further purification. 3,4,5,6-tetrabromo-*ortho*-benzoquinone (*o*-TBBQ) and $[Fe(tren(py)_3)](PF_6)_2$ were synthesized according to previously reported procedures.[1,2] Spectrophotometric grade acetonitrile (MeCN) was purchased from Alfa Aesar and spectrograde acetone was purchased from Jade Scientific. Both were degassed by freeze-pump-thawing before being stored in an Ar-filled drybox.

Synthesis of 2,3-dicyano-p-benzoquinone (DCBQ). 2,3-dicyano-*para*-hydroquinone (1.0 g, 6.2 mmol) was dissolved in glacial acetic acid (12 mL) by heating. In a separate flask, red fuming nitric acid (6 mL) was chilled in an ice bath to which glacial acetic acid (6 mL) was added slowly. The solution of 2,3-dicyano-*para*-hydroquinone was cooled for 5 minutes in an icebath and the red fuming nitric acid/glacial acetic acid solution was added and immediately stirred in an ice bath for 30 minutes. The resulting solution was extracted with dichloromethane (3 x 100 mL), dried with sodium sulfate, and the solvent was removed under reduced pressure. Chloroform (30 mL) was added to the resulting brown residue, refluxed for 30 minutes, and cooled overnight in a freezer. The solid was collected by filtration and washed with cold chloroform and dried overnight in a desiccator. Yield: 65%. The ^{1}H-NMR spectrum matches that reported in the literature (500 MHz, $CDCl_3$, 2H, s, 7.09 ppm).[3] ^{13}C-NMR, 150 MHz, $CDCl_3$, 177.7 ppm, 137.4 ppm, 128.1 ppm, 109.9 ppm. Elemental Analysis Calcd for $C_8H_2N_2O_2$: C, 60.77; H, 1.28; N, 17.72. Found: C, 60.25; H, 1.28; N, 17.48.

Electrochemistry. Electrochemical measurements were collected using a CH instruments model CHI620D electrochemical workstation in an Ar-filled dry box. A standard three-electrode setup was used to determine the reduction potentials of the benzoquinones and the Fe(II/III) oxidation potential for $[Fe(tren(py)_3)](PF_6)_2$ via cyclic voltammetry in acetonitrile and acetone solutions using 0.1 M tetrabutylammonium hexafluorophosphate ($TBAPF_6$) as supporting electrolyte, a Pt disc working electrode, a Ag wire pseudo-reference electrode, and a platinum wire counter electrode. $TBAPF_6$ was purchased from Oakwood Chemical and recrystallized from ethanol twice before use. *o*-TCBQ, *o*-TBBQ, and *p*-TCBQ are referenced internally to the Fc/Fc^+

couple, whereas DDQ and DCBQ potentials are referenced internally to the decamethylferrocene /decamethylferrocenium ($Fc(cp^*)_2/Fc(cp^*)_2^+$) couple, which itself was internally referenced to the ferrocene/ferrocenium (Fc/Fc^+) couple in both MeCN and acetone.

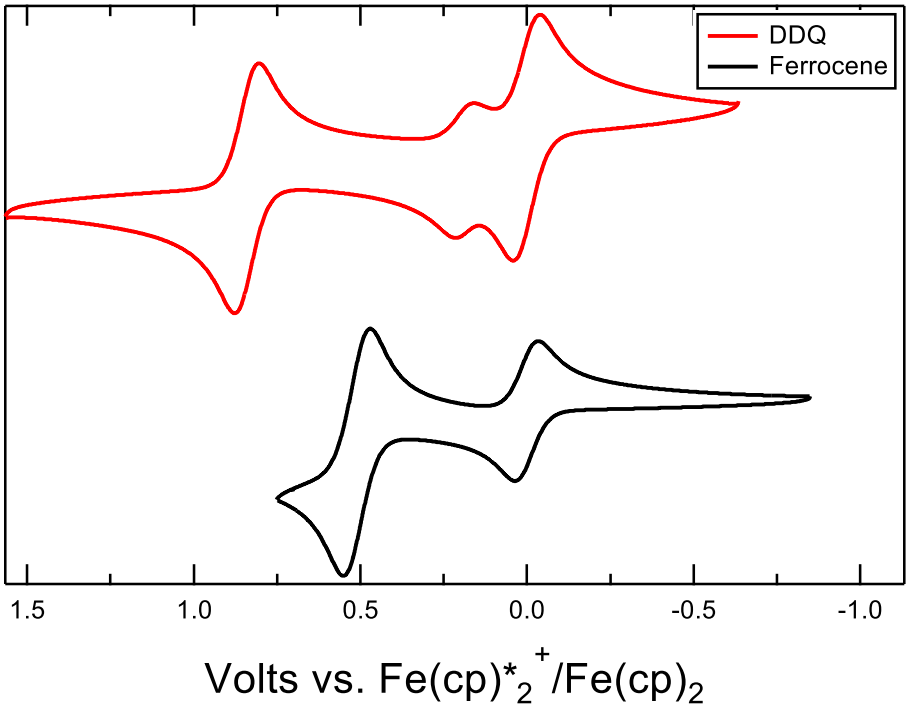

Figure S1. *Cyclic voltammographs of DDQ (red) and ferrocene (black) acquired in MeCN solution.*

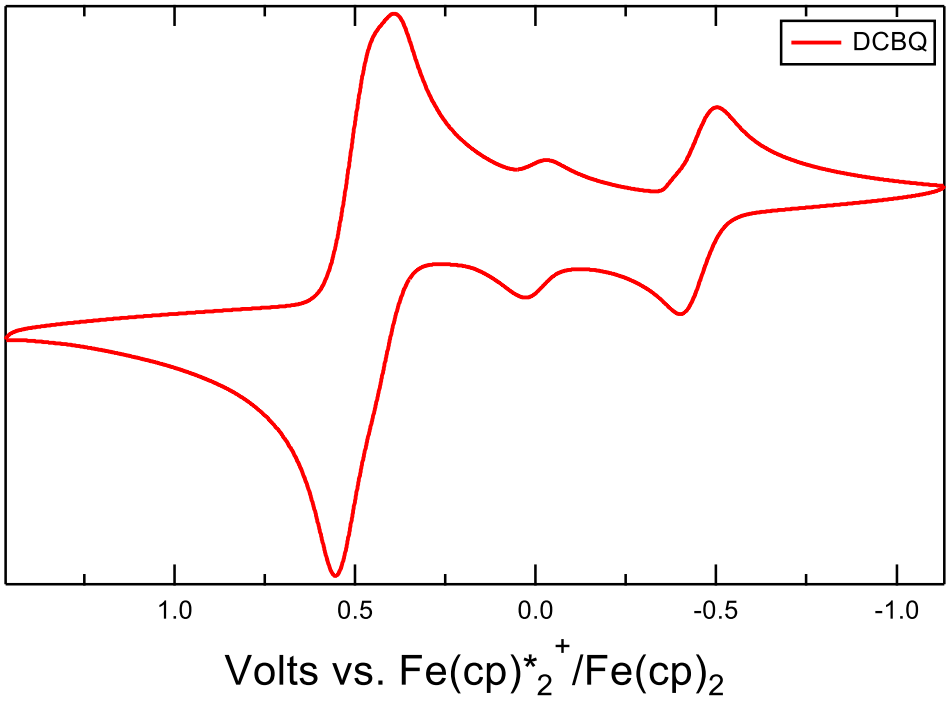

Figure S2. *Cyclic voltammograph of DCBQ acquired in MeCN solution.*

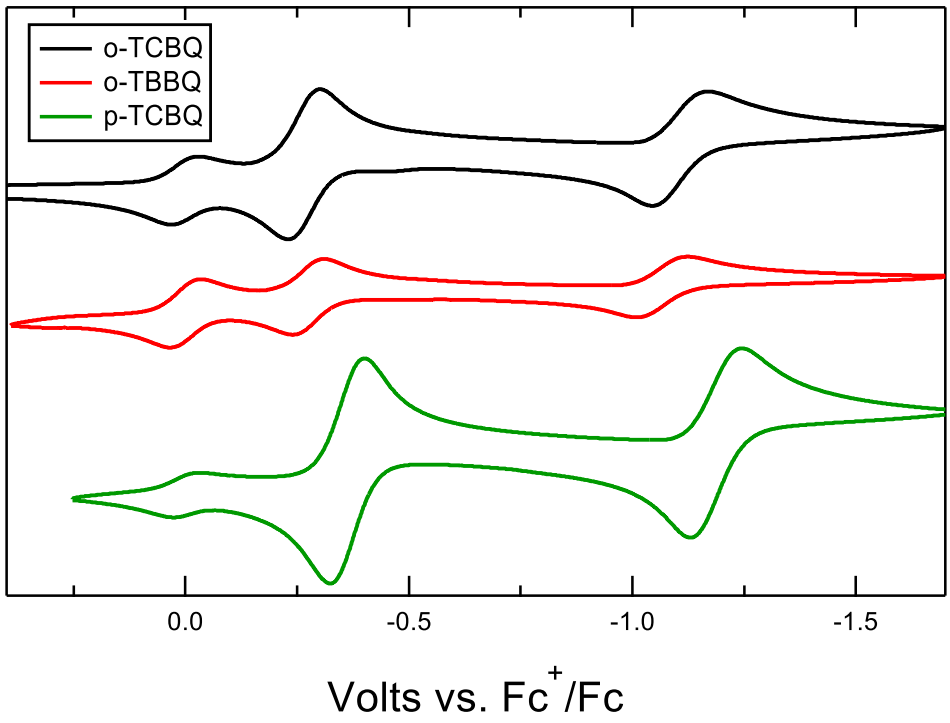

Figure S3. *Cyclic voltammographs of o-TCBQ (black), o-TBBQ (red), and p-TCBQ (green) in MeCN solution.*

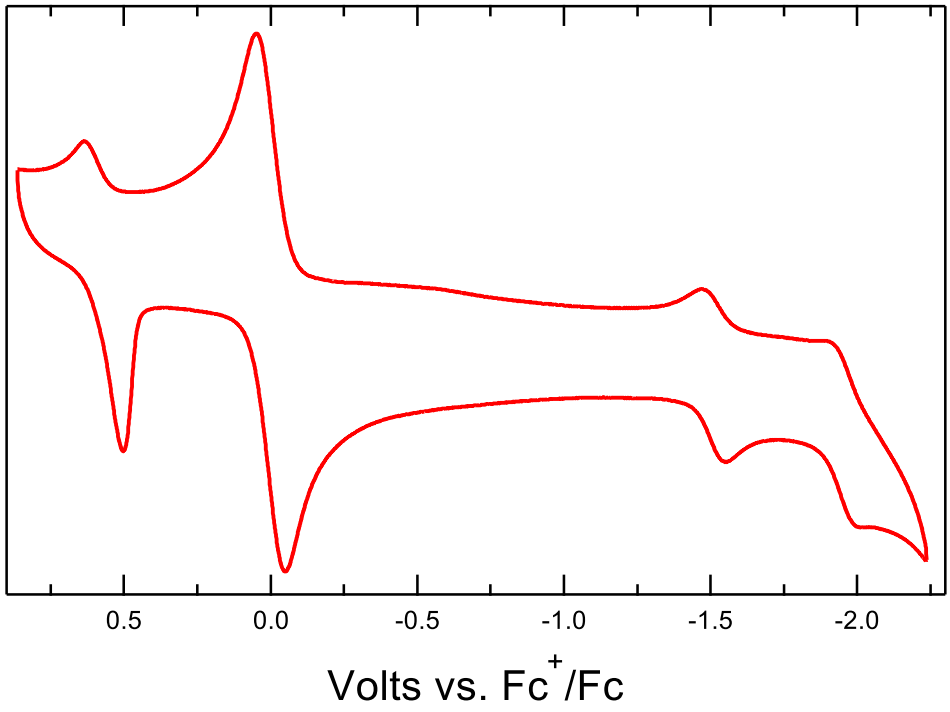

Figure S4. *Cyclic voltammograph of [(Fe(tren(py)$_3$)](PF$_6$)$_2$ in MeCN solution.*

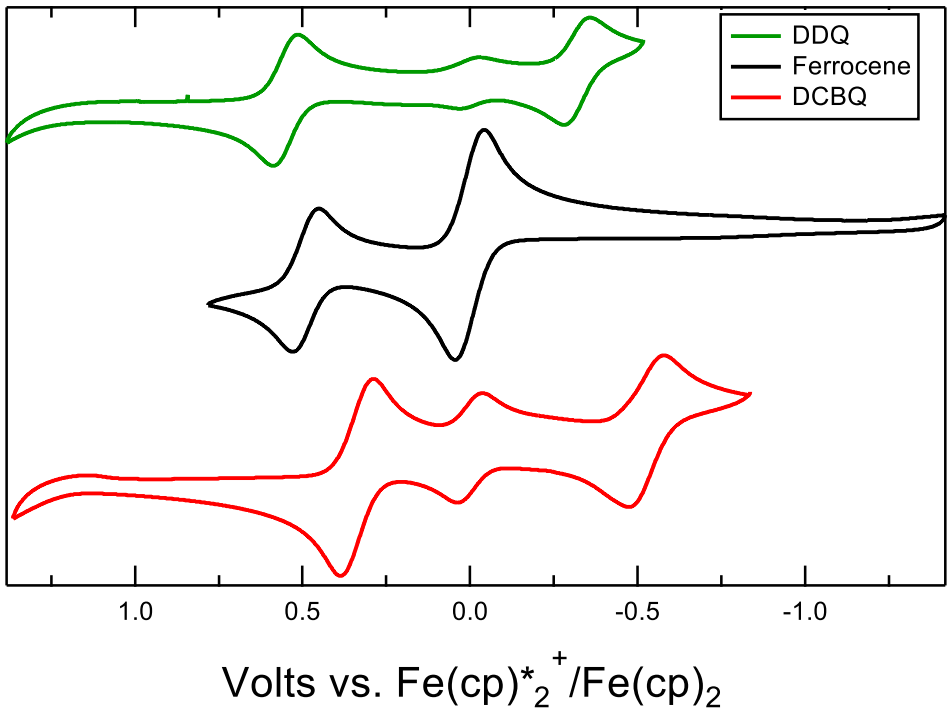

Figure S5. *Cyclic voltammographs of DDQ (green), ferrocene (black), and DCBQ (red) in acetone solution.*

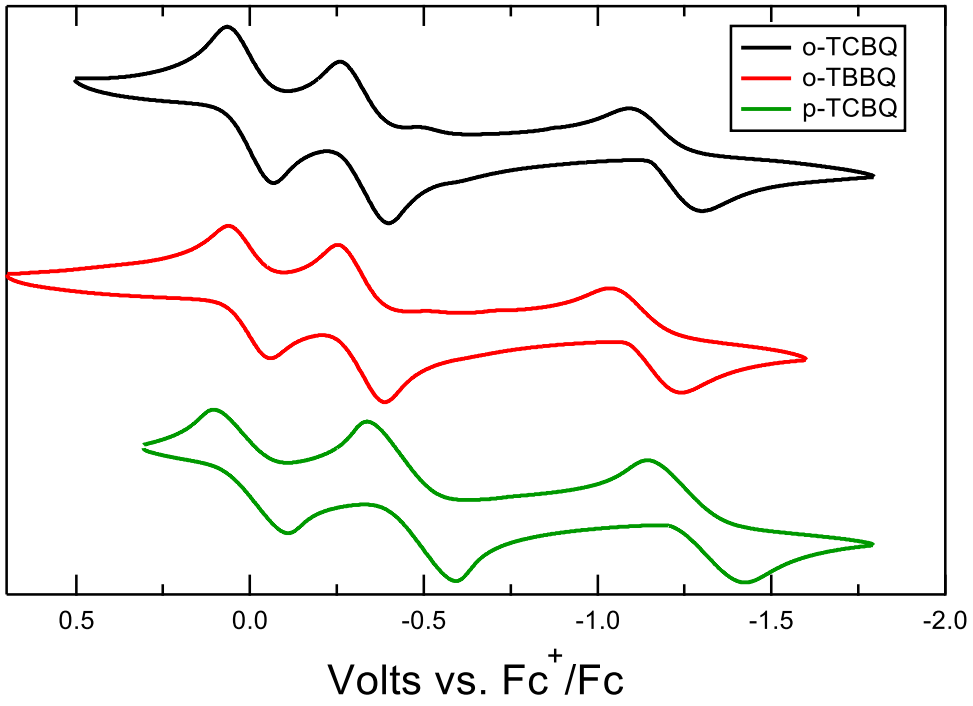

Figure S6. *Cyclic voltammographs of o-TCBQ (black), o-TBBQ (red), and p-TCBQ (green) in acetone solution.*

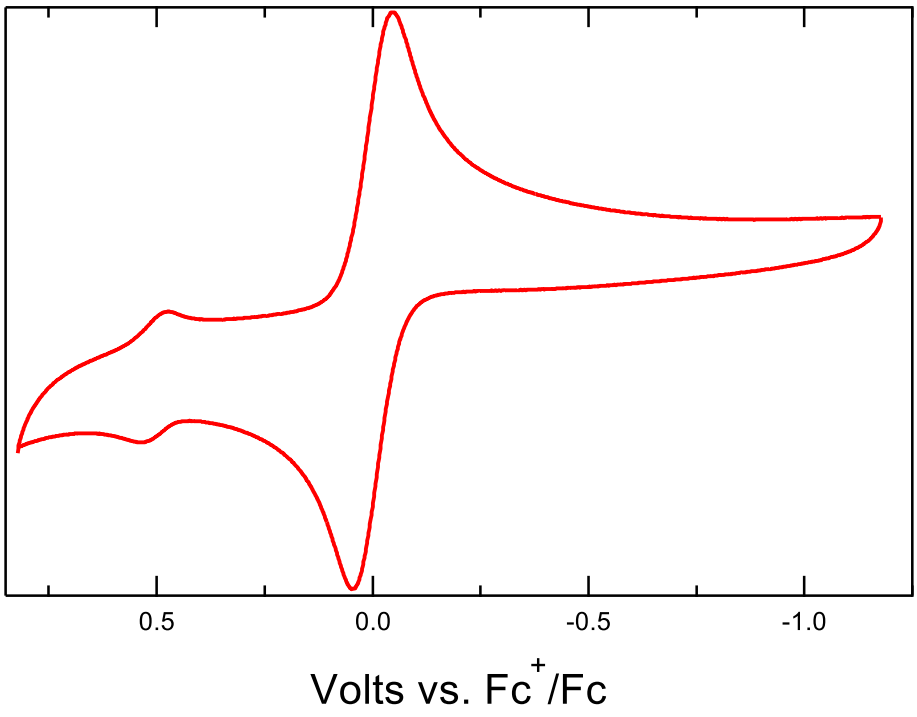

Figure S7. *Cyclic voltammograph of [(Fe(tren(py)$_3$)](PF$_6$)$_2$ in acetone solution.*

Table S1. Summary of reduction potentials of benzoquinones used as quenchers in this study.

	E_{red} (V) vs. Fc/Fc^+	
Compound	MeCN	Acetone
DDQ	0.14	0.07
DCBQ	-0.09	-0.15
o-TCBQ	-0.26	-0.33
o-TBBQ	-0.28	-0.35
p-TCBQ	-0.37	-0.42

Spectroelectrochemistry. UV-Visible spectroelectrochemical experiments were performed in a Pine Instruments electrochemical cell in an Ar-filled dry box. The 1 cm x 1 cm space at the top of the cell held the Ag reference electrode while the Pt working electrode and counter electrode were placed in the 1.7 mm x 10 mm path length window at the bottom of the cell to electrolyze the solution while the absorbance was recorded with SI420 CCD spectrometer. Data were acquired on solutions identical to that just described for the electrochemical measurements, with the exception that solutions of each compound were adjusted to have absorbance values in the range of 0.6 ± 0.1 at the maximum of the lowest energy mid-visible absorption peak. A ground-state absorption spectrum was taken prior to the onset of bulk electrolysis at an over potential of 0.10 V – 0.20 V relative to the reduction potential of the compound.

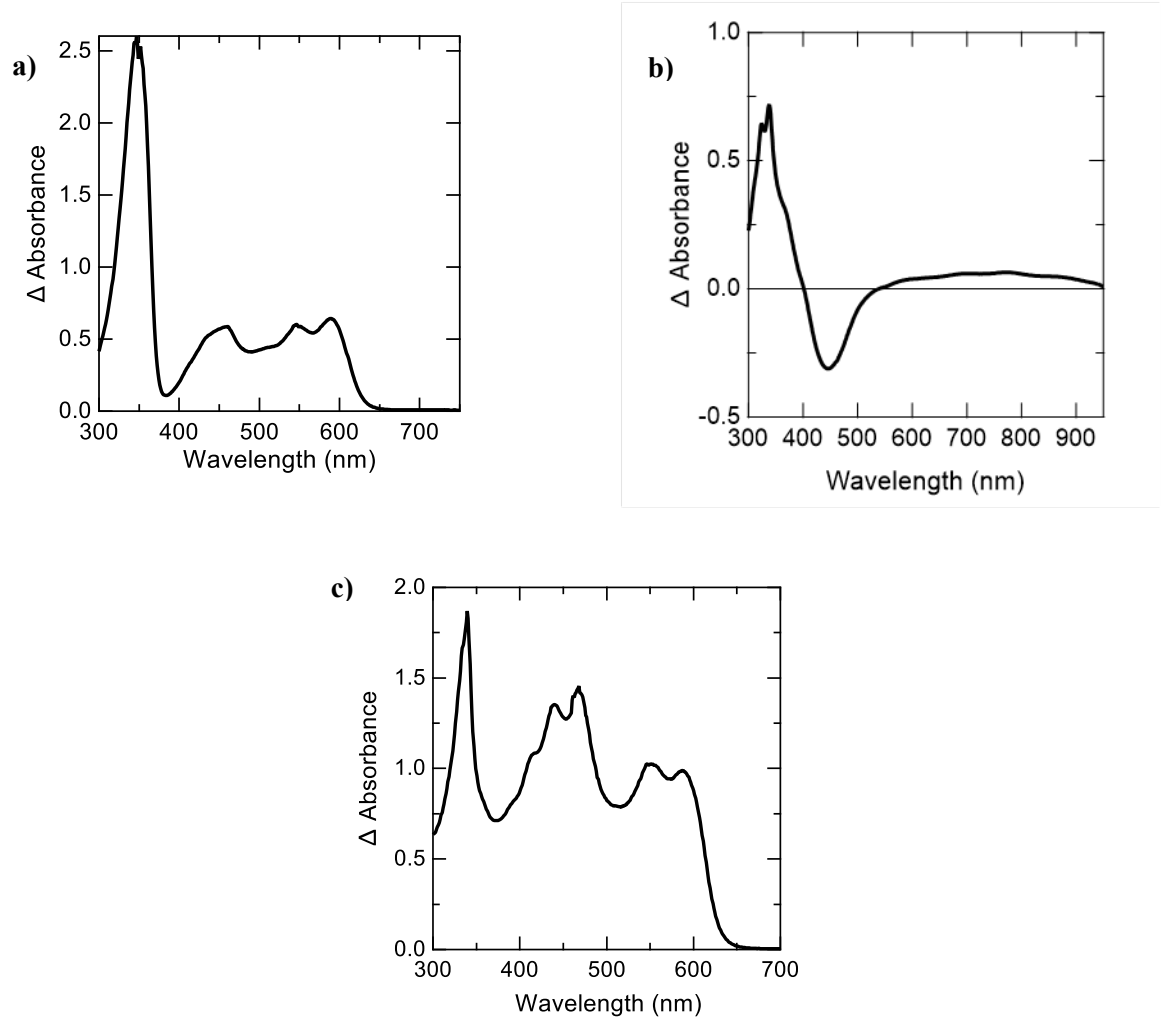

Figure S8. Reductive spectroelectrochemical data for (a) DDQ, (b) o-TCBQ, and (c) DCBQ.

Ground-state and Nanosecond Time-resolved Absorption Spectroscopy. Ground-state electronic absorption spectra were acquired using a Varian 50 UV-Vis electronic absorption instrument. Nanosecond time-resolved absorption data (ns-TA) were acquired using an Edinburgh Instruments LP980 spectrometer fitted with a Hamamatsu R928 photomultiplier tube and interfaced to a Tektronix TDS 3032C oscilloscope. The excitation source was an Opotek Vibrant 355 LD Q-switched Nd:YAG laser. Data were collected at 26 ± 2 ºC (not thermostatted). Samples for Stern-Volmer quenching experiments using $[(Fe(tren(py)_3)](PF_6)_2$ as the sensitizer and the various benzoquinones as quenchers were prepared in an Ar-filled dry-box. A stock solution of $[(Fe(tren(py)_3)](PF_6)_2$ (~ 0.5 mM) and tetrabutylammonium hexafluorophosphate (~0.1 M) was prepared from dry, degassed MeCN or acetone. Varying amounts of quenchers were weighed in 5 ml volumetric flask and 1 mL of the stock solution was added and diluted to give a final Fe(II) MLCT absorption between 0.7- 0.8. Due to slight variations in temperature in the sample compartment, the lifetime of $[(Fe(tren(py)_3)]^{2+}$ was measured after each sample to ensure an accurate k_0/k_{obs} value for the Stern-Volmer plot.

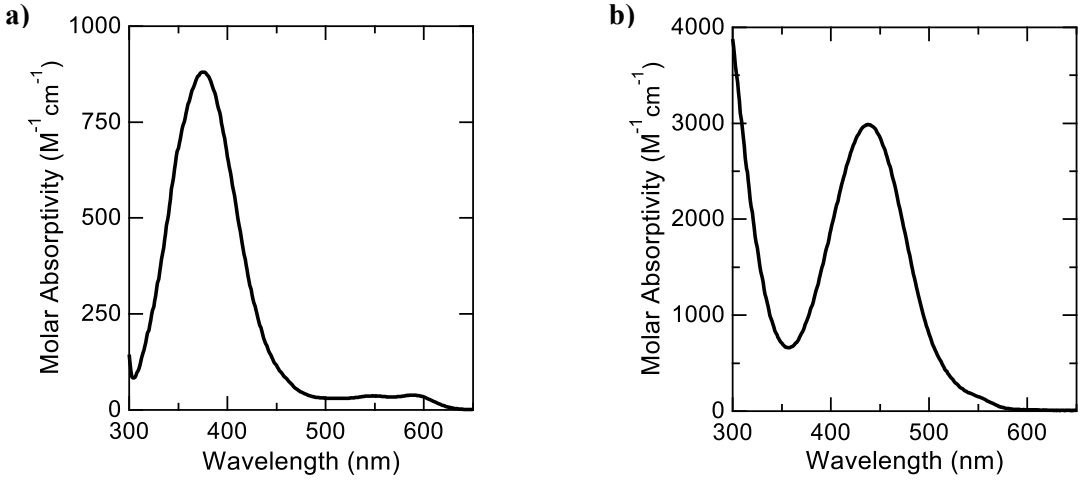

Figure S9. *Electronic absorption spectra of (a) DDQ and (b) o-TCBQ acquired in MeCN solution.*

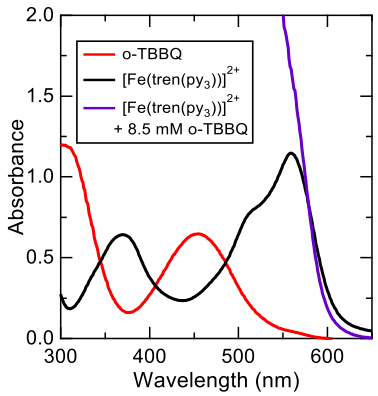

Figure S10. *Electronic absorption spectra of [(Fe(tren(py)$_3$)](PF$_6$)$_2$ (black), o-TBBQ (red) and a solution containing both [(Fe(tren(py)$_3$)[(PF$_6$)$_2$ and o-TBBQ at a concentration of 8.5 mM (purple), all in MeCN solution.*

Nanosecond time-resolved absorption data.

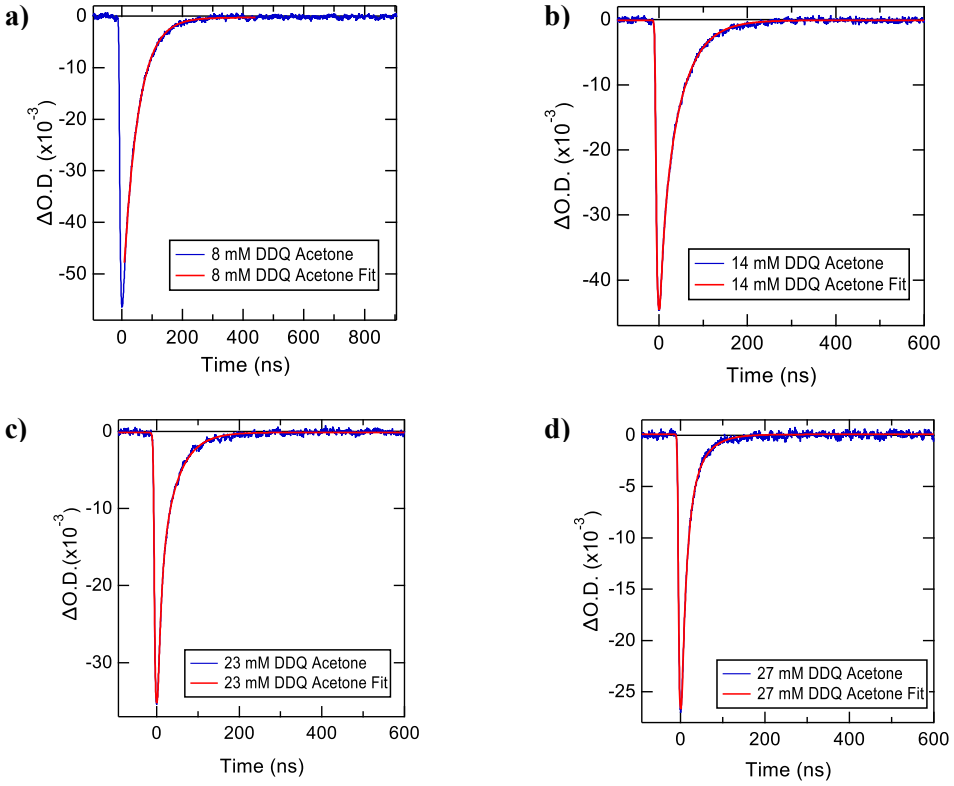

Figure S11. *Quenching studies in acetone solution using [Fe(tren(py)$_3$)]$^{2+}$ following MLCT excitation at 580 nm and probing at 560 nm. (a) 8 mM DDQ, fit with a single exponential (τ_1 = 49 ns) (k_0/k_{obs} = 55 ns/49 ns = 1.12). (b) 14 mM DDQ, fit with bi-exponential Gaussian deconvolution due to contribution from laser scatter (τ_1 = 7 ns, τ_2 = 46 ns), (k_0/k_{obs} = 55 ns/46 ns = 1.2). (c) 23 mM DDQ, fit with bi-exponential Gaussian deconvolution due to contribution from laser scatter (τ_1 = 7 ns, τ_2 = 41 ns), (k_0/k_{obs} = 55 ns/41 ns = 1.34). (d) 27 mM DDQ, fit with bi-exponential Gaussian deconvolution due to contribution from laser scatter (τ_1 = 7 ns, τ_2 = 37 ns), (k_0/k_{obs} = 55 ns/37 ns = 1.48).*

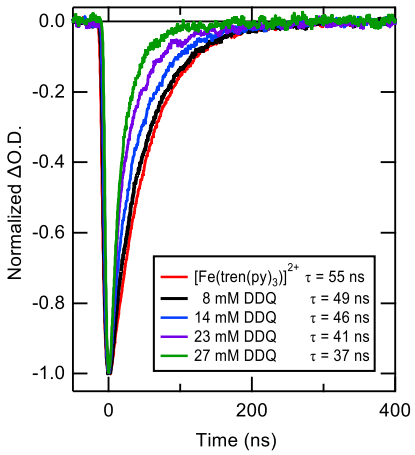

Figure S12. *Normalized overlay of single wavelength kinetics for bimolecular quenching studies with* $[Fe(tren(py)_3)]^{2+}$ *and DDQ in acetone with 0.1M* $TBAPF_6$ (λ_{ex} = 580 nm, λ_{probe} = 560 nm).

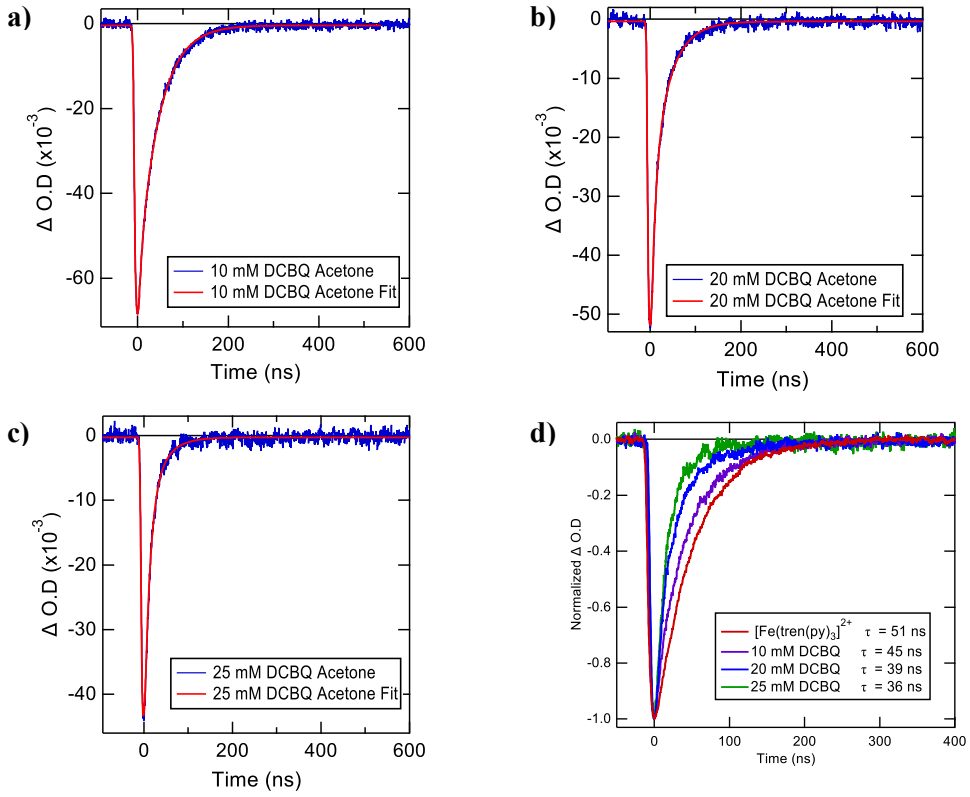

Figure S13. *Quenching studies in acetone solution using* $[Fe(tren(py)_3)]^{2+}$ *following MLCT excitation at 580 nm and probing at 560 nm. (a) 10 mM DCBQ, fit with bi-exponential Gaussian deconvolution due to contribution from laser scatter* (τ_1 = 7 ns, τ_2 = 45 ns), (k_0/k_{obs} = 51 ns/45 ns = 1.13). *(b) 20 mM DCBQ, fit with bi-exponential Gaussian deconvolution due to contribution from laser scatter* (τ_1 = 7 ns, τ_2 = 39 ns), (k_0/k_{obs} = 51 ns/39 ns = 1.3). *(c) 25 mM DCBQ, fit with bi-exponential Gaussian deconvolution due to contribution from laser scatter* (τ_1 = 7 ns, τ_2 = 36 ns), (k_0/k_{obs} = 50 ns/36 ns = 1.38). *(d) Normalized overlay of the data in panels a, b, and c.*

Time-resolved absorption data acquired on solutions containing $[Fe(tren(py)_3)](PF_6)_2$ and 2,3-dichloro-5,6-dicyano-*para*-benzoquinone (DDQ) in acetone are shown in Figures S11 and S12; corresponding data using 2,3-dicyano-*para*-hydroquinone (DCBQ) are shown in Figure S13. Excitation at 580 nm, which corresponds to the $^1A_1 \rightarrow {}^1$MLCT absorption of the iron(II) chromophore, is known to result in the formation of the $^5T_2$ excited state of this compound in ~200 fs.[4] The presence of the $^5T_2$ state is indicated by a bleach feature in the mid-visible region of the spectrum due to the 10-fold attenuation of the intensity of the excited $^5T_2 \rightarrow {}^5$MLCT absorption in this same region.[4b] This lowest-energy excited state of the chromophore relaxes back to the ground state of the molecule via non-radiative decay with an intrinsic lifetime of 55 ± 5 ns.

The data plotted in Figures S11 and S12 reveal a systematic decrease in the lifetime of the $^5T_2$ excited state of $[Fe(tren(py)_3)]^{2+}$ with increasing concentrations of both DDQ and DCBQ, indicating dynamic quenching of the metal-centered excited state by these two acceptors. Since the $^5T_2$ state is non-emissive and Dexter transfer to either a singlet or triplet excited state of the quinone from the $^5T_2$ excited state is spin forbidden,[5] the mechanism of quenching can be directly attributed to an electron transfer process. Furthermore, since formation of a Fe(I) species as well as oxidation of the quinone are not thermodynamically viable under these conditions, electron transfer must result in the oxidation of the excited Fe(II) species and concomitant reduction of the quinone to its semiquinone form. Certain of the data sets suffered from scatter from the excitation source, contributions that were accounted for when necessary by incorporation of a 7 ns component in the kinetic model based on a direct measurement of the instrument response function of the spectrometer.

The results of analogous experiments in which DCBQ is replaced by 3,4,5,6-tetrachloro-*ortho*-benzoquinone (*o*-TCBQ) are shown in Figures S14 - S16. The analysis of these data was complicated due to the fact that the ground-state absorption spectrum of *o*-TCBQ is significantly red-shifted as compared to both DDQ and DCBQ; at concentrations needed to assess the presence (or absence) of quenching of the $^5T_2$ state of $[Fe(tren(py)_3)]^{2+}$, this resulted in significant overlap between the absorption profiles of both chromophores such that excitation of both compounds was unavoidable. The long-lived, positive absorption feature evident in Figures S14b, S14c, and S14d is due to direct excitation of the quinone, a fact verified by time-resolved absorption studies carried out on solutions containing only *o*-TCBQ (Figure S17). The $^5T_2$ state of $[Fe(tren(py)_3)]^{2+}$ is being quenched by the quinone, as evidenced by the reduction in lifetime highlighted in Figure S15. Figure S16 presents data acquired at 610 nm, which is a probe wavelength selective for the excited state of quinone produced via direct excitation. The invariance of the time constant of this feature across the entire range of conditions for which a reduction in the $^5T_2$ lifetime is evident confirms the benign nature of this excited-state species with regard to the chemistry we are probing.

Similar spectral overlap complications arise with the use of 3,4,5,6-tetrabromo-*ortho*-benzoquinone (*o*-TBBQ) (Figures S18-S19). In this case, there is no reduction in the measured lifetime of the $^5T_2$ state of $[Fe(tren(py)_3)]^{2+}$. This is an indication that the $^5T_2$ state of the iron sensitizer is not sufficiently reducing to react with *o*-TBBQ and therefore provides a lower limit on the excited-state reduction potential of this species.

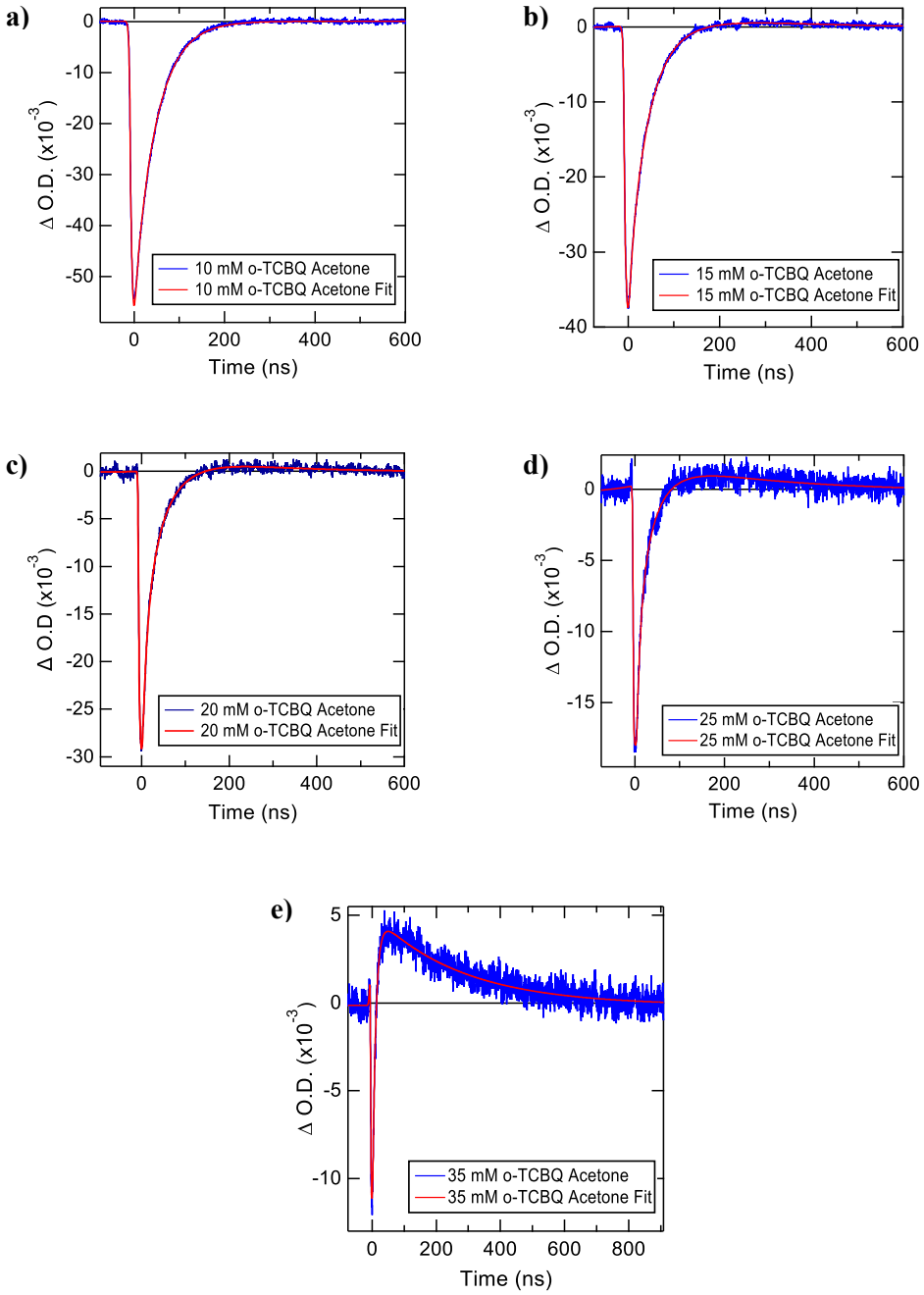

Figure S14. *Quenching studies in acetone solution using $[Fe(tren(py)_3)]^{2+}$ following MLCT excitation at 580 nm and probing at 560 nm. (a) 10 mM o-TCBQ (top left), fit with bi-exponential Gaussian deconvolution due to contribution from laser scatter (τ_1 = 7 ns, τ_2 = 48 ns) (k_0/k_{obs} = 51 ns/48 ns = 1.1). (b) 15 mM o-TCBQ, fit with a tri-exponential Gaussian deconvolution due to contribution from laser scatter and a positive feature (τ_1 = 7 ns, τ_2 = 43 ns, τ_3 = 285 ns) (k_0/k_{obs} = 51 ns/43 ns = 1.18). (c) 20 mM o-TCBQ, fit with tri-exponential Gaussian deconvolution due to contribution from laser scatter and a positive feature (τ_1 = 7 ns, τ_2 = 40 ns, τ_3 = 290 ns), (k_0/k_{obs} = 49 ns/40 ns = 1.23). (d) 25 mM o-TCBQ, fit with a tri-exponential Gaussian deconvolution due to signal contribution from laser scatter and a positive feature (τ_1 = 7 ns, τ_2 = 30 ns, τ_3 = 275 ns). (e) 35 mM o-TCBQ, fit with a tri-exponential Gaussian deconvolution due to signal contribution from laser scatter and a positive feature (τ_1 = 7 ns, τ_2 = 12 ns, τ_3 = 270 ns).*

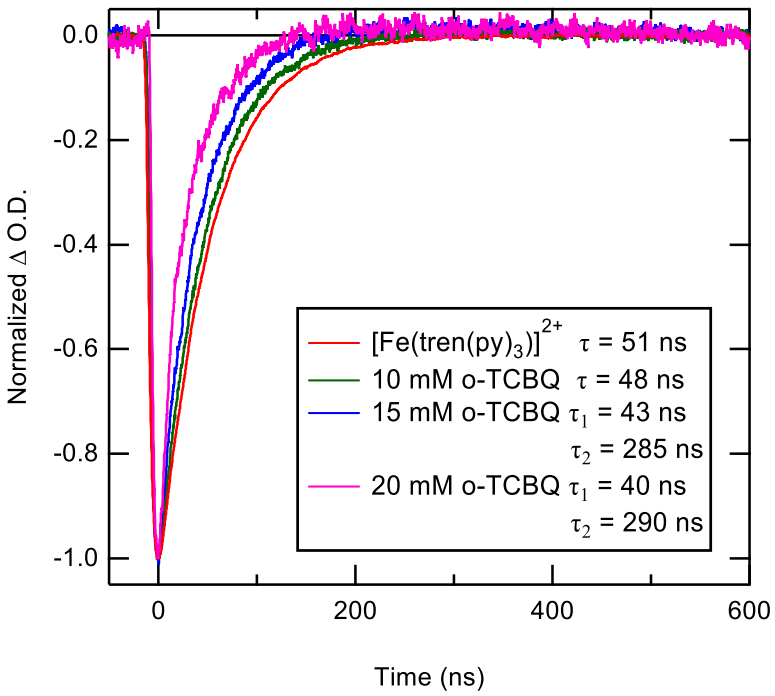

Figure S15. *Normalized overlay of single wavelength kinetics for bimolecular quenching studies between* $[Fe(tren(py)_3)]^{2+}$ *and o-TCBQ in acetone solution with 0.1M* $TBAPF_6$ (λ_{ex} = 580 nm, λ_{probe} = 560 nm).

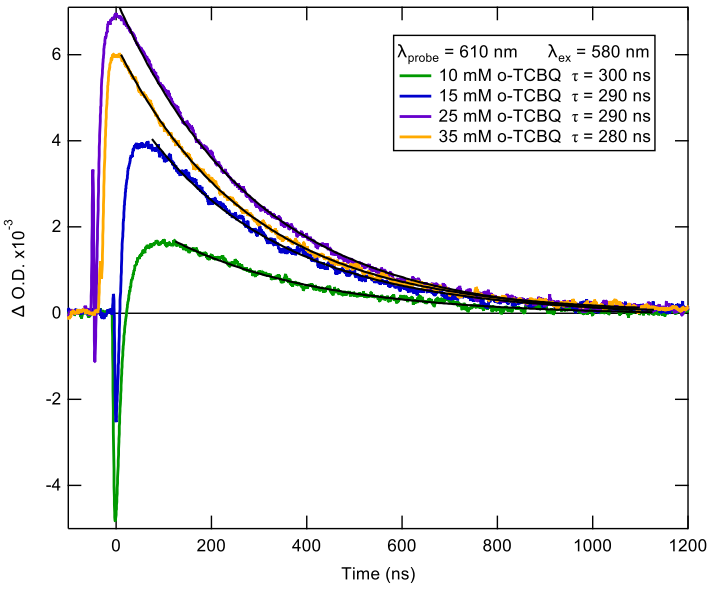

Figure S16. *Single-wavelength nanosecond time-resolved absorption data from quenching studies between* $[Fe(tren(py)_3)]^{2+}$ *and o-TCBQ in acetone solution with 0.1M* $TBAPF_6$. *The data were acquired at* λ_{probe} = 610 nm, *which is selective for the excited state produced upon direct excitation of the quinone.*

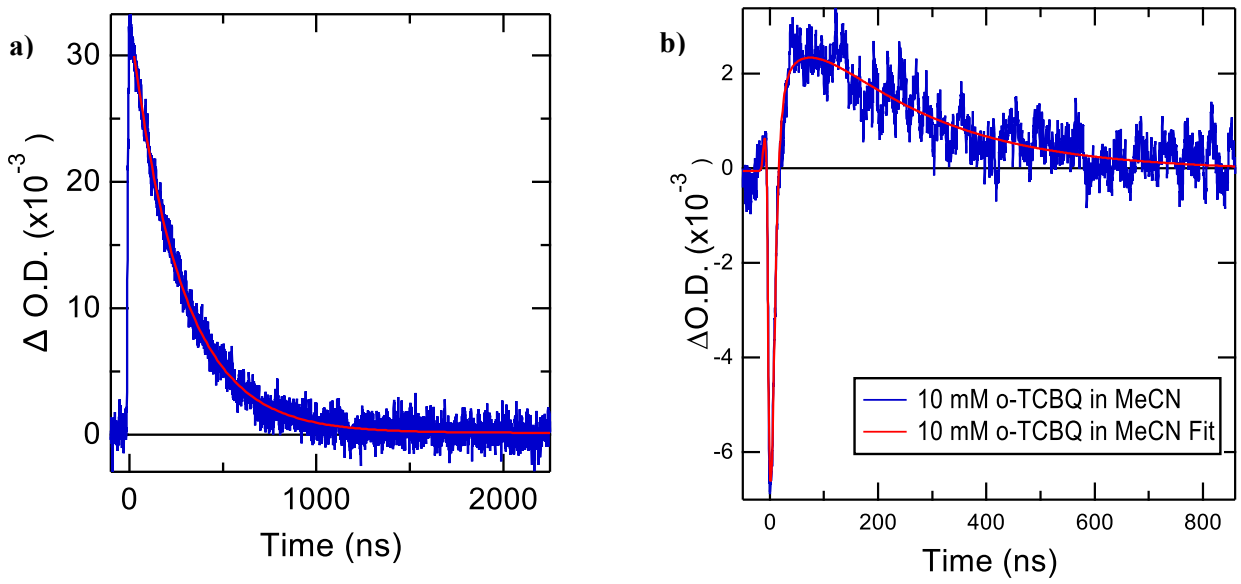

Figure S17. *(a) Transient absorption data acquired on a MeCN solution of o-TCBQ in the absence of* $[(Fe(tren(py)_3)]^{2+}$ *(*λ_{ex} *= 475 nm,* λ_{probe} *= 605 nm). The measured lifetime is* τ *= 270 ns and corresponds to an excited state of o-TCBQ that is produced upon direct excitation of the quinone. (b) Corresponding data collected on a solution 10 mM in o-TCBQ in the presence of* $[(Fe(tren(py)_3)]^{2+}$*(*λ_{ex} *= 580 nm,* λ_{probe} *= 600 nm). The data were fit to a tri-exponential function (including Gaussian deconvolution) with time constants of* τ_1 *= 7 ns (laser scatter),* τ_2 *= 50 ns (slightly quenched* $^5T_2$ *excited state of* $[Fe(tren(py)_3)]^{2+}$*), and* τ_3 *= 225 ns. Given the high degree of correlation among the fitting parameters under these conditions, we believe that the 225 ns component is associated with the same species giving rise to the kinetics shown in (a), i.e. o-TCBQ that has been directly excited due to spectral overlap at this excitation wavelength.*

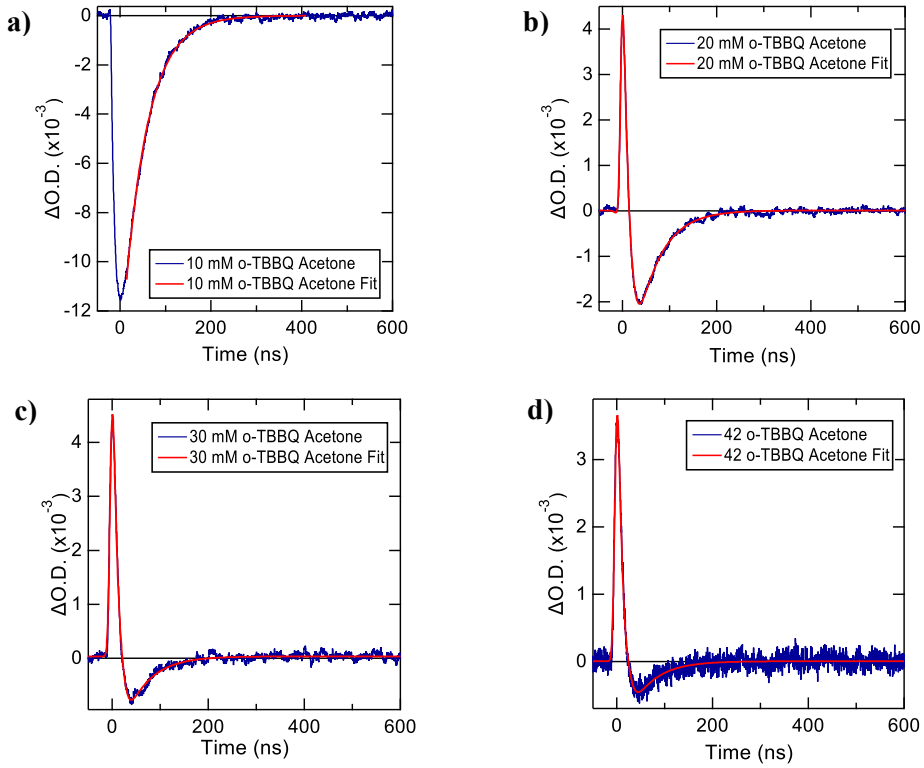

Figure S18. *Quenching studies in acetone solution using $[Fe(tren(py)_3)]^{2+}$ following MLCT excitation at 580 nm and probing at 560 nm. (a)10 mM o-TBBQ, fit with a single exponential (τ_1 = 50 ns).(b) 20 mM o-TBBQ, fit with bi-exponential Gaussian deconvolution due to significant signal from the positive feature due to partial excitation of o-TBBQ (τ_1 = 7 ns, τ_2 = 50 ns). (c) 30 mM o-TBBQ, fit with bi-exponential Gaussian deconvolution due to significant signal from the positive feature due to partial excitation of o-TBBQ (τ_1 = 7 ns, τ_2 = 50 ns). (d) 42 mM o-TBBQ, fit with bi-exponential Gaussian deconvolution due to significant signal from the positive feature due to partial excitation of o-TBBQ (τ_1 = 7 ns, τ_2 = 50 ns).*

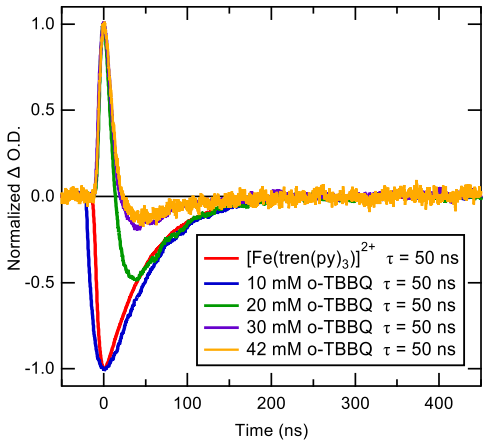

Figure S19. *Normalized overlay of single wavelength kinetics acquired for bimolecular quenching studies with $[Fe(tren(py)_3)]^{2+}$ and o-TBBQ in acetone with 0.1M $TBAPF_6$ (λ_{ex} = 580 nm, λ_{probe} = 560 nm).*

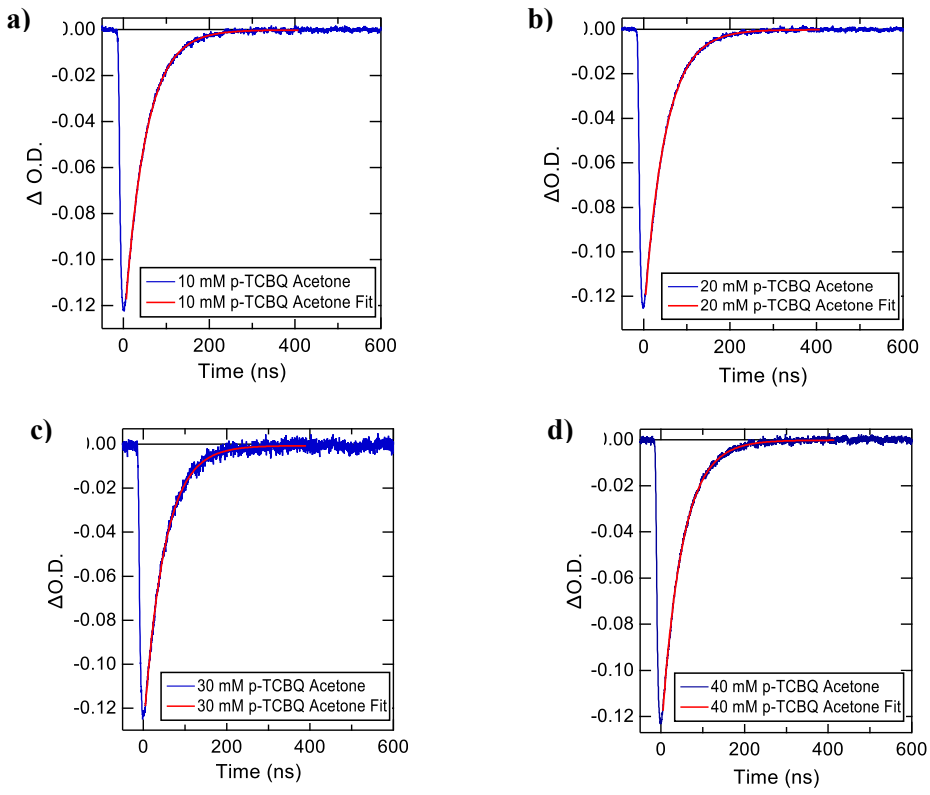

Figure S20. *Quenching studies in acetone solution using $[Fe(tren(py)_3)]^{2+}$ following MLCT excitation at 580 nm and probing at 560 nm. (a) 10 mM p-TCBQ, fit with a single exponential (τ_1 = 50 ns). (b) 20 mM p-TCBQ, fit with a single exponential (τ_1 = 50 ns). (c) 30 mM p-TCBQ, fit with a single exponential (τ_1 = 50 ns). (d) 40 mM p-TCBQ, fit with a single exponential (τ_1 = 50 ns).*

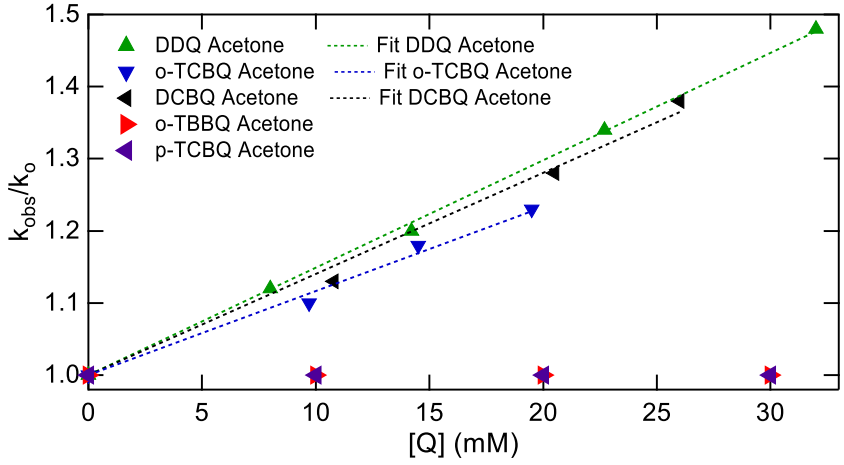

Figure S21. *Stern-Volmer plot of transient absorption data of quenching studies carried out in acetone solution between $[Fe(tren(py)_3)]^{2+}$ and the quinone acceptors indicated, using the data presented in Figures S11, S13, S14, S18, and S20.*

Analogous measurements were also carried out in acetonitrile solutions. Figures S22 - S25 present the additional supporting data not depicted in Figure 3. The IRF was found to vary slightly more with the MeCN solution than that observed with acetone but was still within an acceptable range.

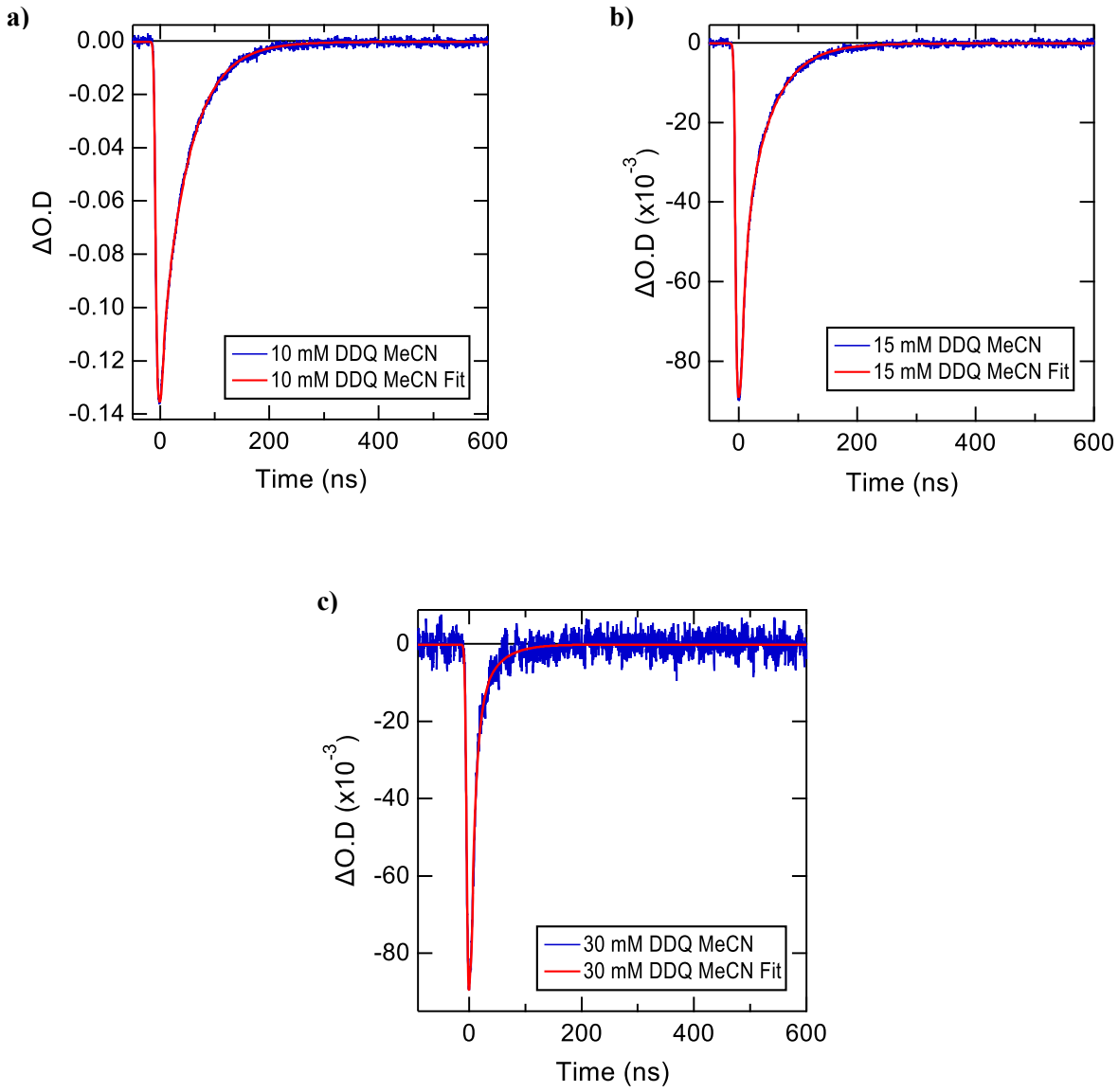

Figure S22. *Quenching studies in acetonitrile solution using $[Fe(tren(py)_3)]^{2+}$ following MLCT excitation at 580 nm and probing at 560 nm.(a) 10 mM DDQ, fit with bi-exponential Gaussian deconvolution due to contributions from laser scatter (τ_1 = 5 ns, τ_2 = 50 ns), (k_0/k_{obs} = 55 ns/50 ns = 1.1). (b) 15 mM DDQ, fit with bi-exponential Gaussian deconvolution due to contributions from laser scatter (τ_1 = 6 ns, τ_2 = 45 ns), (k_0/k_{obs} = 55 ns/45 ns = 1.22). (c) 30 mM DDQ, fit with bi-exponential Gaussian deconvolution due to contributions from laser scatter (τ_1 = 8 ns, τ_2 = 34 ns), (k_0/k_{obs} = 49 ns/34 ns = 1.44).*

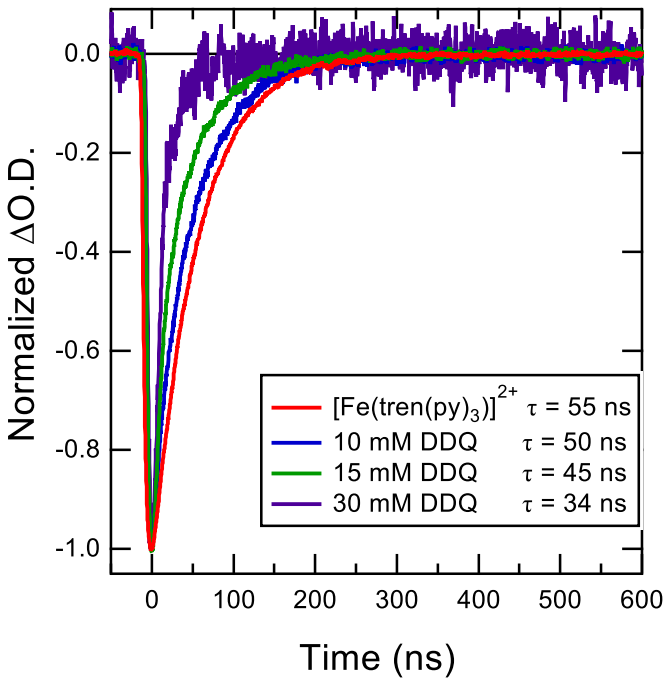

Figure S23. *Normalized overlay of single wavelength kinetics acquired for bimolecular quenching studies with* $[Fe(tren(py)_3)]^{2+}$ *and DDQ in acetonitrile with 0.1M* $TBAPF_6$ (λ_{ex} = 580 nm, λ_{probe} = 560 nm).

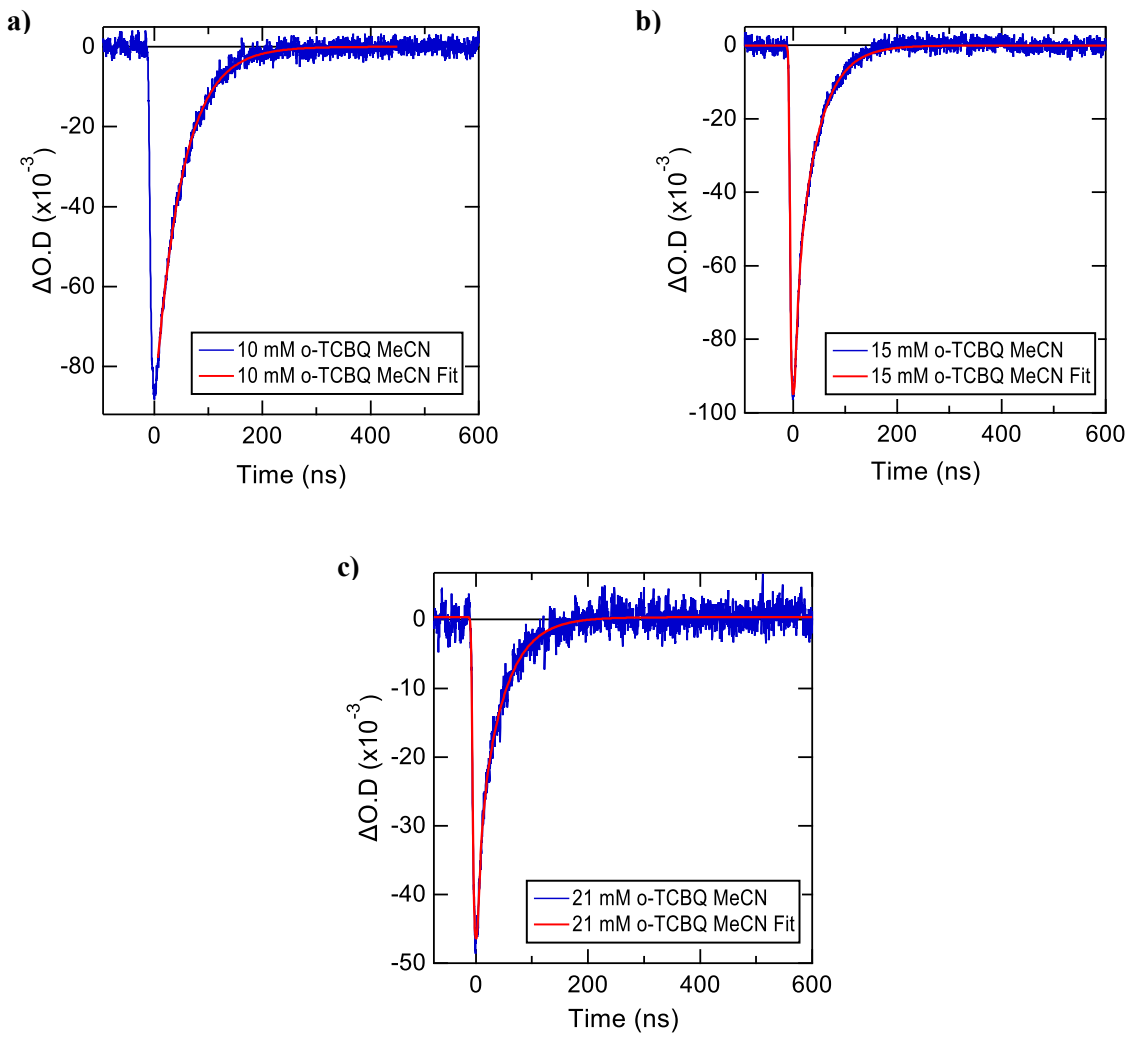

Figure S24. *Quenching studies in acetonitrile solution using* $[Fe(tren(py)_3)]^{2+}$ *following MLCT excitation at 580 nm and probing at 560 nm. (a) 10 mM o-TCBQ, fit with a single exponential (*τ_1 *= 50 ns), (*k_0/k_{obs} *= 55 ns/50 ns = 1.1). (b) 15 mM o-TCBQ, fit with bi-exponential Gaussian deconvolution due to contributions from laser scatter (*τ_1 *= 7 ns,* τ_2 *= 42 ns), (*k_0/k_{obs} *= 50 ns/42 ns = 1.19). (c) 21 mM o-TCBQ, fit with bi-exponential Gaussian deconvolution due to significant signal contribution from laser scatter (*τ_1 *= 7 ns,* τ_2 *= 44 ns), (*k_0/k_{obs} *= 55 ns/44 ns = 1.25).*

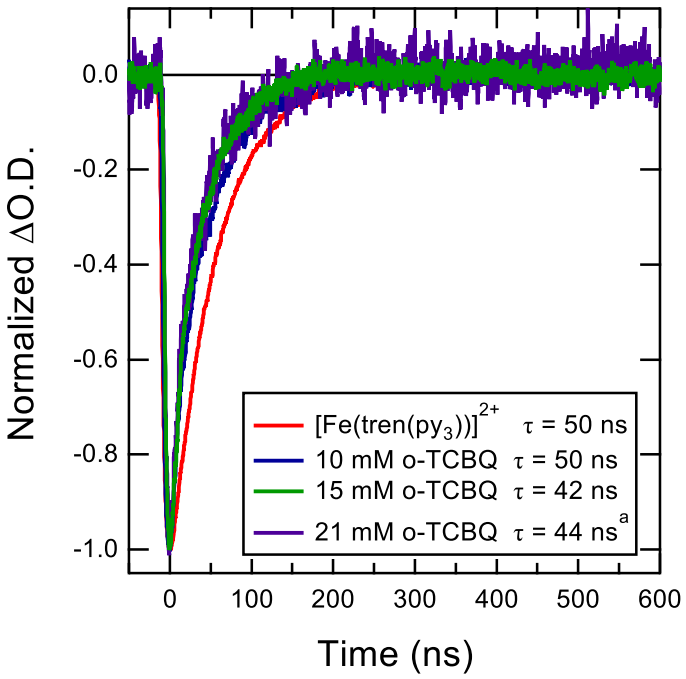

Figure S25. *Normalized overlay of single wavelength kinetics acquired for bimolecular quenching studies with* $[Fe(tren(py)_3)]^{2+}$ *and o-TCBQ in acetonitrile with 0.1M* $TBAPF_6$ (λ_{ex} = 580 nm, λ_{probe} = 560 nm)(a = *The longer lifetime at higher quencher concentration is a result of measuring a 55 ns lifetime for* $[Fe(tren(py)_3)]^{2+}$ *at the time of the experiment, as mentioned above).*

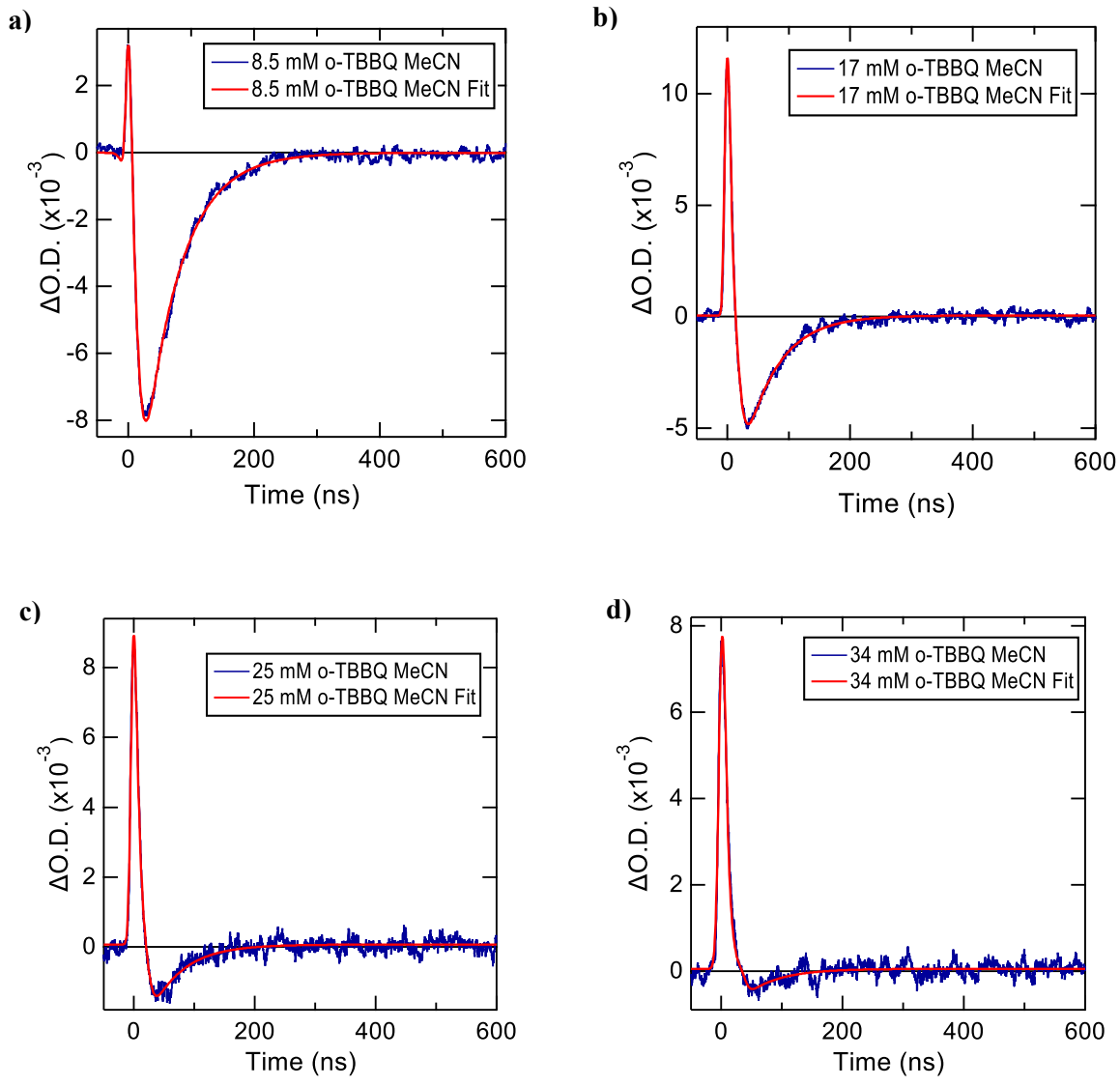

Figure S26. *Quenching studies in acetonitrile solution using $[Fe(tren(py)_3)]^{2+}$ following MLCT excitation at 580 nm and probing at 560 nm. (a) 8.5 mM o-TBBQ, fit with bi-exponential Gaussian deconvolution due to signal from the positive feature resulting from direct excitation of o-TBBQ (τ_1 = 7 ns, τ_2 = 55 ns). (b) 17 mM o-TBBQ, fit with bi-exponential Gaussian deconvolution due to signal from the positive feature resulting from direct excitation of o-TBBQ (τ_1 = 7 ns, τ_2 = 55 ns). (c) 25 mM o-TBBQ, fit with bi-exponential Gaussian deconvolution due to signal from the positive feature resulting from direct excitation of o-TBBQ (τ_1 = 7 ns, τ_2 =55 ns). (d) 34 mM o-TBBQ, fit with bi-exponential Gaussian deconvolution due to signal from the positive feature resulting from direct excitation of o-TBBQ (τ_1 = 7 ns, τ_2 =55 ns).*

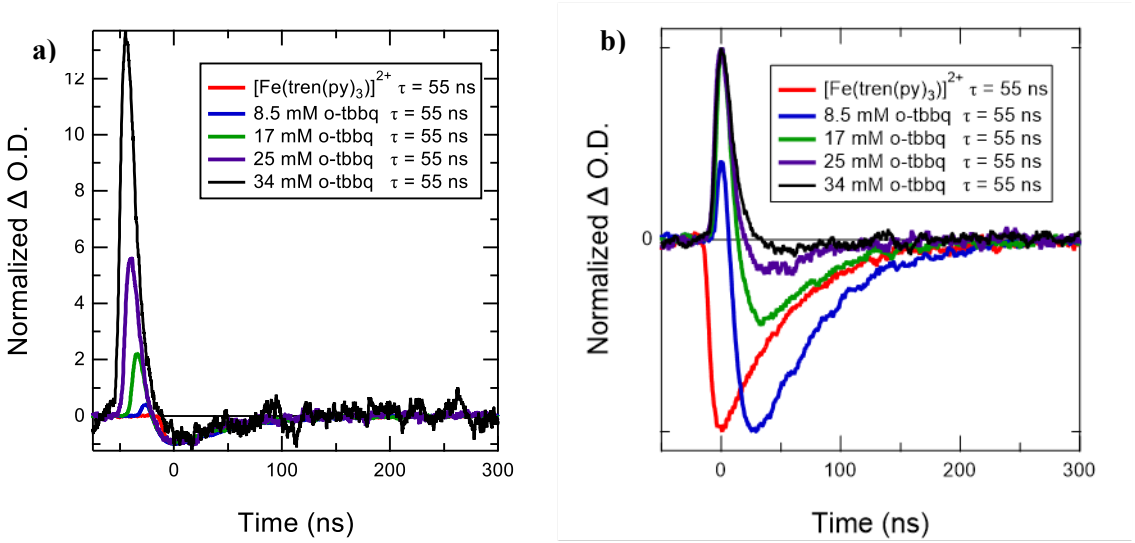

Figure S27. *Normalized overlay of single wavelength kinetics acquired for bimolecular quenching studies with* $[Fe(tren(py)_3)]^{2+}$ *and o-TBBQ in acetonitrile with 0.1M* $TBAPF_6$ (λ_{ex} = 580 nm, λ_{probe} = 560 nm). *(a) Normalized to the bleach maximum to clearly show the indifference in the excited state lifetime. (b) Normalized to the most positive or negative peak maximum.*

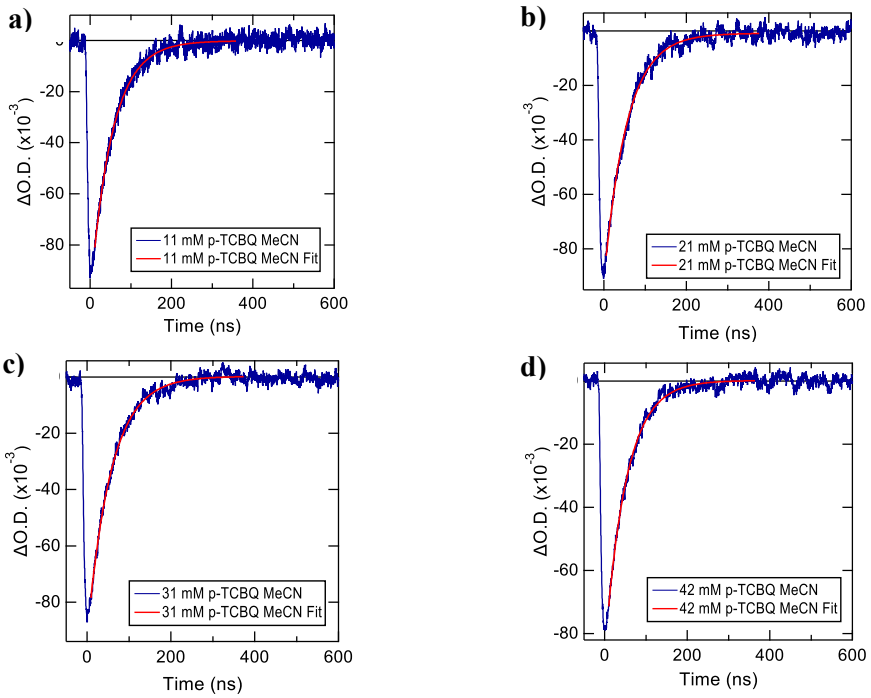

Figure S28. *Quenching studies in acetonitrile solution using $[Fe(tren(py)_3)]^{2+}$ following MLCT excitation at 580 nm and probing at 560 nm. (a) 11 mM p-TCBQ, fit with a single exponential (τ_1 = 55 ns). (b) 21 mM p-TCBQ, fit with a single exponential (τ_1 = 55 ns). (c) 31 mM p-TCBQ, fit with a single exponential (τ_1 = 55 ns). (d) 42 mM p-TCBQ, fit with a single exponential (τ_1 = 55 ns).*

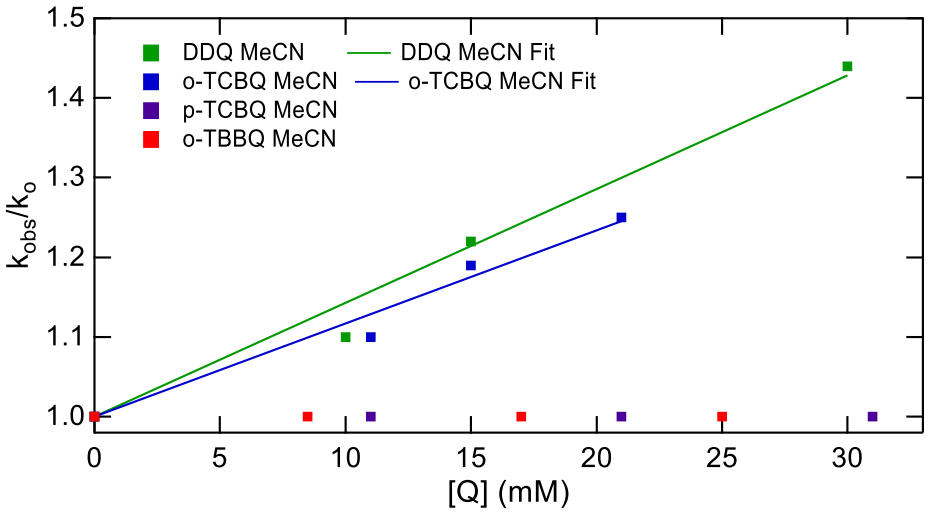

Figure S29. *Stern-Volmer plot of transient absorption data of quenching studies carried out in acetonitrile solution with 0.1M $TBAPF_6$ between $[Fe(tren(py)_3)]^{2+}$ and the quinone acceptors indicated, using the data presented in Figures S22-S28.*

Table S2. Reduction Potentials and Quenching rate constants for Quenchers in acetonitrile with 0.1M $TBAPF_6$.

Quencher	E_{red} (V) vs. Fc/Fc^+	k_q ($M^{-1}s^{-1}$)	ΔG (V)
DDQ	0.14	2.6×10^5	-0.44
DCBQ	-0.09	a	-0.18
o-TCBQ	-0.26	2.1×10^5	-0.01
o-TBBQ	-0.28	-	0.01
p-TCBQ	-0.37	-	0.10

a = DCBQ was not soluble in MeCN at the desired concentrations and quenching data was not collected.

References.

(1) (a) Jackson, C. L.; Koch, W. On Certain Derivatives of ortho-benzoquinone. *American Chemical Journal* 1901, 26, 10-46. (b) Jackson, C. L.; Porter, H. C. *American Chemical Journal* **1903**, *30*, 523.

(2) Struch, N.; Topić, F.; Schnakenburg, G.; Rissanen, K.; Lüyzen, A. Electron-Deficient Pyridylimines: Versatile Building Blocks for Functional Metallosupramolecular Chemistry. *Inorg. Chem.* **2018**, *57*, 241-250. DOI: 10.1021/acs.inorgchem.7b02412

(3) Lyu, H.; Jafta, C. J.; Popovs, I.; Meyer, H. M.; Hachtel, J. A.; Huang, J.; Sumpter, B. G.; Dai, S.; Sun, X. G. A dicyanobenzoquinone based cathode material for rechargeable lithium and sodium ion batteries. *J. Mater. Chem. A.* **2019**, *7*, 17888-17895. DOI: 10.1039/c9ta04869c/c9ta04869c.

(4) (a) Monat, J.E.; McCusker, J.K. Femtosecond Excited-State Dynamics of an Iron(II) Polypyridyl Solar Cell Sensitizer Model. *J. Am. Chem. Soc.* **2000**, *122*, 4092-4097. (b) Smeigh, A.L.; Creelman, M.; Mathies, R.A.; McCusker, J.K. Femtosecond Time-Resolved Optical and Raman Spectroscopy of Photo-induced Spin-Crossover: Temporal Resolution of Low Spin-to-High Spin Optical Switching. *J. Am. Chem. Soc.* **2008**, *130*, 14105-14107. (c) Huse, N.; Kim, T.K.; Jamula, L.; McCusker, J.K.; de Groot, F.M.F.; Schoenlein, R.W. Photo-induced Spin-State Conversion in Solvated Transition Metal Complexes Probed by Time-resolved Soft X-Ray Spectroscopy. *J. Am. Chem. Soc.* **2010**, *132*, 6809-6816. (d) Huse, N.; Cho, H.; Hong, K.; Kim, T.K.; Jamula, L.; de Groot, F.M.F.; McCusker, J.K.; Schoenlein, R.W. Femtosecond Soft X-Ray Spectroscopy of Solvated Transition Metal Complexes: Deciphering the Interplay of Electron and Structural Dynamics. *J. Phys. Chem. Lett.* **2011**, *2*, 880-884.

(5) Guo, D.; Knight, T.E.; McCusker, J.K. Angular Momentum Conservation in Dipolar Energy Transfer. *Science* **2011**, *334*, 1684-1687.